Mechanical Dither Design for Ring Laser Gyroscope

Dong-Chan Lee*, Gun Moon, Jae-Cheul Lee
Center for Photonics & Communications, Institute for Advanced Engineering, Kyunggi-do 449-863, Korea

The gyroscopes have been used as a suitable inertial instrument for the navigation guidance and attitude controls. The accuracy as very sensitive sensor is limited by the lock-in region (dead band) by the frequency coupling between two counter-propagating waves at low rotation rates. This frequency coupling gives no phase difference and an angular increment is not detected. This problem can be overcome by the mechanical dithering. The purpose of the mechanical dithering is to suppress the dead band, oscillate the monoblock about the rotation axis and add an external rotation rate. This paper presents the theoretical considerations of the mechanical performances of dither on the basis of the loading condition and angular characteristics due to the piezoelement deformation and the validity of theoretical equations are compared through FEM (Finite Element Method) simulations.

Key Words : Ring Laser Gyroscope, Lock-in Region, Dead Band, Dither, Resonant Frequency, Torsional Stiffness, Peak Angular Amplitude, Peak Dither Rate

1. Introduction

When there is an applied rotation about the axis normal to the plane of rotation, the operation of gyroscope depends on the phase difference for beams traveling in opposite direction within a closed path. This difference gives rise to a phase difference. But the accuracy of gyroscopes have been limited by the lock-in region due to the fact that at low rotation rates of gyroscope the frequency coupling mechanism arises from backscattering of the mirrors. This effect gives no phase difference and hence no detect of angular increment. In other words, this reduces the angular sensitivities to the electrical and mechanical disturbances such as low frequency noise components, in the optical measurement. It is important to minimize the transition periods of lock-in region. The dithering motion is to operate the gyroscope about the lock-in threshold in order to be sensitive against input rotation rates which are below that certain threshold (Fig. 1).

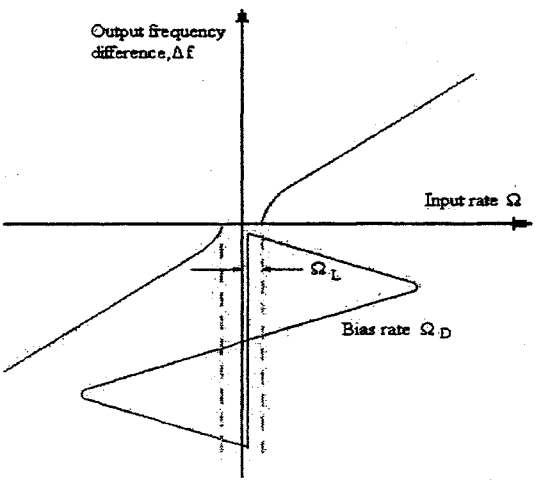

Fig. 1 Alternating bias technique in ring laser gyroscope

The purpose of the mechanical dithering is to suppress the dead band, oscillate the block about the rotation axis and add an external rotation rate. The followings are described about the

* Corresponding Author,
E-mail : dclee@iae.re.kr
TEL : +82-31-330-7553; **FAX** : +82-31-330-7113
Center for Photonics & Communications, Institute for Advanced Engineering, Kyunggi-do 449-863, Korea.
(Manuscript **Received** July 23, 2001; **Revised** January 11, 2002)

design considerations.

The systematic considerations for the gyroscope;
- Structural resonant frequency
- Peak angular amplitude and peak dither rate
- Mechanical properties of spoke material (choice of material)
- Driving technique
- Inertia of dithered components

The considerations for the mechanical performance;
- Torsional stiffness
- Bending profile
- Points of inflection
- Stress induced by bending of the spokes

The detailed considerations for the spoke;
- Geometry of spokes
- Number of spokes
- Attachment of dither mechanism to solid block and inertial reference frame

The mechanical dither design was explained by Shackleton B. R. in 1987. His paper presented the geometrical approach of spoke, but had no considerations of the loading condition and angular characteristics due to the piezoelement deformation. In this paper, the mechanical performances of dither are theoretically presented on the basis of the loading condition and angular characteristics due to the piezoelement deformation. And using the transverse vibration behavior of elastic spoke, the resonant frequency of mechanical dither is calculated. Through the finite element analysis, it is shown that the mechanical dither can effectively be evaluated.

The recent dithering method uses the electrical signal processing for the low backscatter in conjunction with a stable gas discharge, a suitable dither drive and a stabilized resonator cavity length. But the simplest dithering method is to use the mechanical dither.

2. Theoretical Consideration

The spoke shown in Fig. 2 undergoes transverse vibration and small elastic bending deformation due to alternate piezoelement deformation. The spoke end has the inertial effect of solid block system through bush. Using Newton's second law, the equation of motion of spoke can be derived as follows. Figure 3(a) shows a portion of member undergoing transverse motion and Fig. 3(b) shows a small free body diagram.

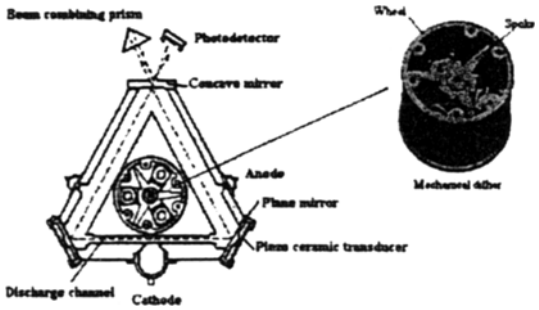

Fig. 2 Schematic model of ring laser gyroscope

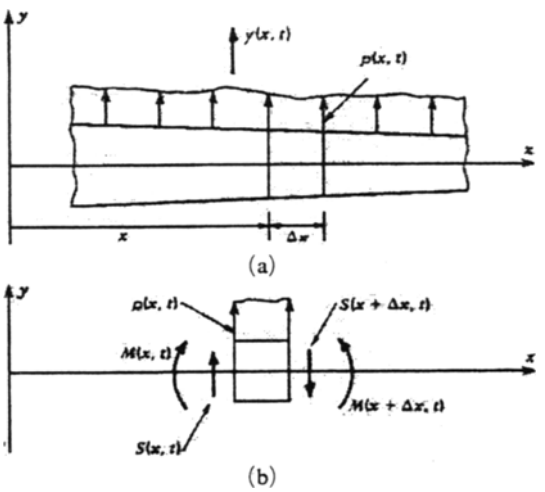

Fig. 3 Member undergoing transverse vibration

In Fig. 3, $y(x, t)$ is the transverse motion of the points on the neutral axis of the beam, $M(x, t)$ is the bending moment, $S(x, t)$ is the transverse shear force, and $p(x, t)$ is the external force per unit length. The spoke will be assumed as Bernoulli-Euler beam. And it will be assumed that the rotatory inertia of beam may be neglected in the moment equation. The equations of motion for the mass Δm in the above free body diagram may be derived using Newton's laws. Thus,

$$\sum F_y = (\Delta m)\, a_y \tag{1}$$

$$\sum M_G = (\Delta I_G)\, \ddot{\theta} \tag{2}$$

where G is the mass center of Δm and $\ddot{\theta}$ is the angular acceleration. However, it was previously stated that rotatory inertia would be neglected in the moment equation, so Eq. (2) reduces to

$$\sum M_G=0 \tag{3}$$

For a linearly small elastic beam, if the slope $\partial y/\partial x$ of beam remains small, the curvature may be approximated by $\partial^2 y/\partial x^2$. Thus the bending moment is approximated by,

$$M(x,\ t)=EI\frac{\partial^2 y}{\partial x^2} \tag{4}$$

where I is the moment of inertia of the cross section from the neutral axis Applying Eqs. (1) and (3) to the free body diagram, we obtain

$$-\frac{\partial S}{\partial x}+p(x,\ t)=\rho A\frac{\partial^2 y}{\partial t^2} \tag{5}$$

$$S=\frac{\partial M}{\partial x} \tag{6}$$

Combining Eqs. (4), (5) and (6), we get

$$\frac{\partial^2}{\partial x^2}\left(EI\frac{\partial^2 y}{\partial x^2}\right)+\rho A\frac{\partial^2 y}{\partial t^2}=p(x,\ t) \tag{7}$$

For the fundamental deformation of spoke in the free vibration, it may be assumed as,

$$EI\frac{\partial^4 y}{\partial x^4}+\rho A\frac{\partial^2 y}{\partial t^2}=0 \tag{8}$$

where $y(x,\ t)=Y(x)\cos(\omega t+\psi)$ (9)

Using a separation of variables approach, the characteristic equation is given by

$$\frac{d^4 Y}{dx^4}-\lambda^4 Y=0 \tag{10}$$

where, $\lambda^4=\dfrac{\rho A\omega^2}{EI}$ (11)

The general solution of Eq. (10) for the deformation mode may be written in the following form

$$Y(x)=c_1\sinh\lambda x+c_2\cosh\lambda x+c_3\sin\lambda x+c_4\cos\lambda x \tag{12}$$

It is assumed that the spoke of mechanical dither is clamped at one end and a lumped mass is attached at the other end of spoke. The spoke has no deflection and slope at the clamped end. But the boundary condition of the mass-attached end is as follows. Since the particle has no rotatory inertia at the mass-attached end, $M(L,\ t)$ is zero from Eqs. (3). And applying Eq. (1) and (6) to the mass-attached end, the boundary conditions is given by,

$$\frac{\partial}{\partial x}\left(EI\frac{\partial^2 y}{\partial x^2}\right)\Big|_{x=L}=m\frac{\partial^2 y}{\partial t^2}\Big|_{x=L} \tag{13}$$

Equation (13) shows that the transverse force at $x=L$ depends on the inertial effect of solid monoblock. But if the behavior of the mass-attached end is taken into account by the inertia of solid monoblock and working condition(feasible angular velocity 2.26~2.61rad./sec, feasible resonant frequency 380Hz~400Hz), $\partial^3 y/\partial x^3$ in the lefthand side term may be approximated to zero. In other words, the elastic deformation effect of spoke due to piezoelement is greater than the inertia of monoblock. Thus the boundary conditions of deformation mode is given by,

$$Y(0)=0,\ \frac{dY}{dx}\Big|_{x=0}=0,\ \frac{d^2Y}{dx^2}\Big|_{x=L}=0,\ \frac{d^3Y}{dx^3}\Big|_{x=L}\approx 0 \tag{14}$$

From the above boundary conditions, we obtain the following equations.

$$\begin{bmatrix} 0 & 1 & 0 & 1 \\ \lambda & 0 & \lambda & 0 \\ \lambda^2\sinh\lambda L & \lambda^2\cosh\lambda L & -\lambda^2\sin\lambda L & -\lambda^2\cos\lambda L \\ \lambda^3\cosh\lambda L & \lambda^3\sinh\lambda L & -\lambda^3\cosh\lambda L & \lambda^3\sin\lambda L \end{bmatrix}\begin{Bmatrix} c_1 \\ c_2 \\ c_3 \\ c_4 \end{Bmatrix}=\begin{Bmatrix} 0 \\ 0 \\ 0 \\ 0 \end{Bmatrix} \tag{15}$$

In order to have a nontrivial solution, the determinant of the coefficients must vanish. This leads to the characteristic equation,

$$\cos\lambda L\cosh\lambda L=-1 \tag{16}$$

From Eq. (16), (λL) may be given by,

$$(\lambda L)_n\approx\frac{2n-1}{2}\pi,\ n=1,\ \cdots,\ n \tag{17}$$

The natural frequency of elastic spoke is given from Eq. (11) and (17).

$$\omega_n=(\lambda L)_n^2\sqrt{\frac{EI}{mL^3}} \tag{18}$$

From Eq. (18), is the mass distribution about the neutral axis which passes through the center as shown Fig. 3(b). The mass moment of inertia per unit length $J(x)$ is related to $I(x)$, given by

$$J(x)=\rho I(x)=\frac{m(x)}{A(x)}I(x)=\kappa(x)^2 m(x) \quad (19)$$

where ρ is the mass density and $\kappa(x)$ is the radius of gyration about the neutral axis. For the lumped mass of solid block system, the mass moment of inertia J_i may be given by

$$J_i=\sum m_i\kappa_i^2 \quad (20)$$

Taking into account Eqs. (18) and (20) and neglecting an own mass of elastic elements in comparison with a mass of solid block system, the mass applied to spoke can be given by,

$$m=\frac{J_m}{nL'^2} \quad (21)$$

where J_m is a moment of inertia of the solid block system, n is a number of driving spoke and L' is the fixing point of solid monoblock on the spoke.

Using Eqs. (18) and (21), the natural frequency is rewritten to,

$$\omega_n=2\pi f_n=(\lambda L)_n^2\sqrt{\frac{nEIL'^2}{J_mL^3}} \quad (22)$$

where L is a working elastic length of spoke. From Eq. (25), the difference of vibration mode of dither spoke depends on the numerical factor $(\lambda L)_n$.

3. Driving Load Description

The deformation of spoke in Fig. 2 is under the alternate deformation of piezoelement on both face A-B and face C-D. The opposite voltage signals on two elements are loaded and result in the compression and expansion on the piezoelement along the direction of spoke length. The bimorph elastic piezoelement and the deformed shape of spoke due to the piezoelement deformations are shown in Fig. 4.

The spoke undergoes a very small deformation under the piezoelement loading, in comparison with thickness, width and span of spoke. Because the deformation will be sufficiently small, we can use the coordinates of the undeformed cross-section in order to provide an adequate approximation to the location of the point after deformation. Thus if IJ and MN in the undeformed beam of Fig. 4 are deformed into concentric circular arcs I_1J_1 and M_1N_1, we assume that the difference between their radii of curvature can still be taken as . Since $IJ=I_1J_1=M_1N_1$ from the definition of neutral axis, the strain of I_1J_1 is given by,

$$\varepsilon_x=\frac{I_1J_1-IJ}{IJ}=\frac{I_1J_1-M_1N_1}{M_1N_1}=-\frac{y}{R}$$
$$=-\frac{d\phi}{ds}y \quad (23)$$

where ϕ is the deflection angle of bending beam.

From the stress-strain relationship, the longitudinal normal stress σ_x is given by,

$$\sigma_x=E\varepsilon_x=-E\frac{y}{R}=-E\frac{d\phi}{ds}y \quad (24)$$

By the equilibrium requirements, the bending stress σ_x along the longitudinal can be rewritten into,

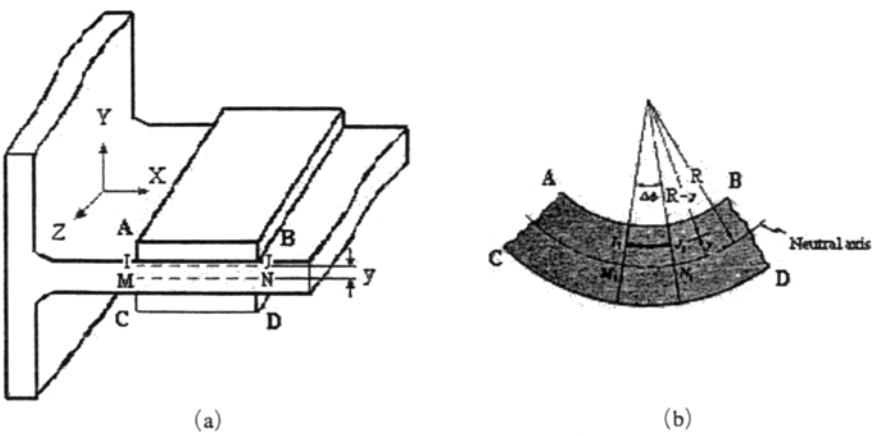

(a) (b)

Fig. 4 Deformation of piezoelement under bending moment

$$\sigma_x = -\frac{M_b y}{I_{zz}} \tag{25}$$

where I_{zz} is the moment of inertia of the area about the neutral axis.

From Eqs. (24) and (25), the longitudinal strain ε_x and the pure bending moment are given by,

$$\varepsilon_x = \frac{1}{E}\left(-\frac{M_b y}{I_{zz}}\right),\ M_b = -\frac{EI_{zz}}{y}\varepsilon_x \tag{26}$$

Setting the maximum strain into $\varepsilon_x \approx \Delta L / L_0$ at the piezoelement $(y = d/2)$, the bending moment due to the piezoelement may be given by,

$$M_b = -\frac{2EI_{zz}}{d}\left(\frac{\Delta L}{L_0}\right) \tag{27}$$

on the neutral axis, where L_0 is the length of piezoelement, d is the thickness of spoke and ΔL is the maximum stretched length of piezoelement along the spoke length.

For an arbitrary point x in $a < x < L$, the vertical deflection δ_x under a moment M_i and a load P_i may be given by,

$$EI\delta_x = EI\delta_0 + EI\delta_0' x + \sum_i \frac{M_i a_{mi}(2x - a_{mi})}{2} + \sum_i \frac{P_i a_{pi}^2 (3x - a_{pi})}{6} \tag{28}$$

where a_{mi} is the location of a moment M_i and a_{pi} is the location of a load P_i on the spoke.

For the clamped end,

$$\delta_0 = \delta_0' = 0 \tag{29}$$

Using the third and fourth terms in Eq. (28), if we assume that the maximum deflection due to bending moment and applied force is equal at the mass attached end, the equivalent vertical force P is given by,

$$\delta_{\max} = \frac{Pa^2}{6EI_{zz}}(3L - a) = \frac{M_b}{EI_{zz}} L_0 (L - a_1) \tag{30}$$

$$P = \frac{6M_b (L - a_1) L_0}{a^2 (3L - a)} \tag{31}$$

From Eqs. (27) and (31), the bending angle θ_a at the loading point a is approximated as the peak angular amplitude.

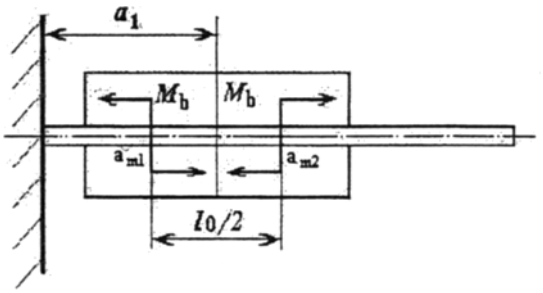

Fig. 5 Behavior of piezoelement

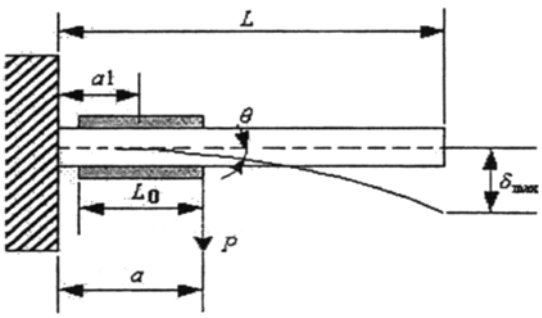

Fig. 6 Equivalent force due to bending moment

$$\theta_a = \frac{Pa^2}{2EI_{zz}} = \frac{3M_b (L - a_1) L_0}{EI_{zz}(3L - a)} = \frac{6}{d}\frac{L - a_1}{3L - a}\Delta L \tag{32}$$

From the condition that the maximum external work is equal to the maximum kinetic energy, the peak dither rate is given by,

$$U_{\max} = T_{\max}$$

$$\frac{1}{2} p\delta_a = \frac{1}{2}\left(\frac{J_m}{n}\right)\dot{\theta}_{\max}^2$$

$$\dot{\theta}_{\max} = \frac{(L - a_1)\Delta L}{(3L - a)\, d}\sqrt{\frac{48nEI}{aJ_m}} \tag{33}$$

where δ_a is the vertical deflection at the loading point a.

4. Simulation

Using the above equations, the resonant frequency of mechanical dither can be estimated by the geometrical parameters. As the examples of simulation, the ring laser gyroscope is shown in Fig. 7. The components of solid block system are considered as the dummy inertia, except the mechanical dither.

The primary goal of the finite element analysis is a guide for the structural design of the geometrically complicated dither. The structural behaviors of mechanical dither take into account two aspects: the first is the resonant frequency and the deformation mode, and the second is the peak dither rate within the dithering range.

This radial dither is mounted to the solid block of gyroscope and to the inertial reference frame via the wedge-shaped spokes. The bending moment of spoke due to the driving deformation of piezoelement ($\Delta L = \pm 2\mu m$) may be calculated from Eq. (27). From Fig. 2, the geometric parameters of spoke are as follows: $n=4$, $L=$ 14.25mm, $L'=10.50$mm, $w=30.00$mm, $a=$ 6.25mm, $a_1=4.00$mm. If the deformation of spoke due to the driving moment and the resonant frequency are fundamentally given, the equivalent polar mass moment of inertia of the dithering system (J_m) may be given by,

$$J_m = \frac{K_\theta}{(2\pi f_n)^2} = \frac{M_b}{(2\pi f_n)^2 \theta_0} \tag{34}$$

The equivalent polar mass moment of inertia is numerically 1.66×10^{-3}kg/m^2 from Eq. (34), based on the test resonant frequency. The structural damping factor was given as *Q−factor* ($Q=1/2\zeta$) through the test, which is 150. The material of mechanical dither is *INVAR 36 ALLOY*. Figure 7 shows the components of ring laser gyroscope. The magnetic core and coil are used for sensing the angular velocity of rotating monoblock system.

For the finite element model, the peak dither rate and resonant frequency are simulated through the frequency response analysis, using MSC/NASTRAN V70. 5. Table 1 shows the results of the simulations and test.

In Table 1, the results of the finite element analyses and numerical solutions show that the maximum relative errors to test results are within 2 % in the resonant frequency and 5 % in the peak dither rate, and two methods are relatively valid for designing the mechanical dither. The relative error between finite element analyses and numerical solutions depend on the working elastic length as shown in Eq. (22), (31), (32) and (33). This working elastic length may be the effective bending length under the bending deformation of a spoke.

5. Conclusion

From the general flexural beam mechanism, the mechanical performances of dither can be found and the geometrical parameters and mate-

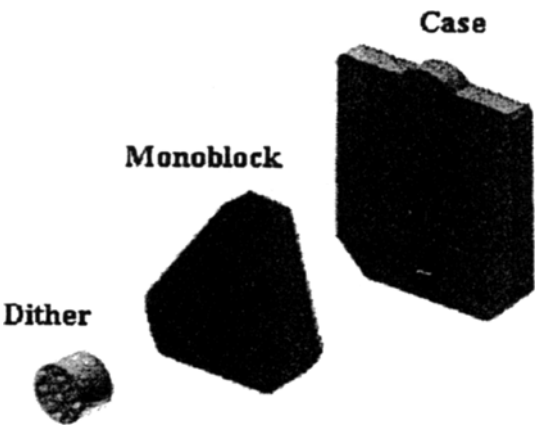

Fig. 7 Components of monoblock system in ring laser gyroscope

Table 1 Comparison of resonant frequencies for the mechanical dithers

No	*Thickness D (mm)*	*Test* *Frequency (Hz), Peak dither rate (deg/sec)*	*FEM* *Frequency (Hz), Peak dither rate (deg/sec)*	*Numerical Eq.* *Frequency (Hz), Peak dither rate (deg/sec)*
1	2.94	362.00, 134.15	359.54, 137.25	356.07, 137.19
2	3.08	383.00, 149.10	381.23, 141.61	381.80, 144.24
3	3.22	400.00, 150.00	405.01, 143.52	404.13, 147.49

rial properties are used for the estimation of the mechanical characteristics such as torsional stiffness, bending profile, stress caused by bending of the spokes, peak dither rate and resonant frequency. And since the stress within spoke and piezoelectric element may further limit the peak angular amplitude and the peak dither rate, the peak dither rate is usually limited to the range which does not cause stresses in the spoke material to exceed the effective material stress.

The effective bending length as the working elastic length is the important parameter which has an influence on the angular deflection. But the geometrical parameters of spoke can approximately be used. And the finite element analysis can be used for designing the concrete and complicated spoke within the given design range.

Acknowledgement

This study is supported by Korean Ministry of Science & Technology through National Research Laboratory Program (No. 2000-N-NL-01-C-253)

References

Alexander Chajes, 1990, *Structural Analysis*, Prentice-Hall, 2nd edition.

Ansel C. Ugural and Saul K. Fenster, 1995, *Advanced Strength and Applied Elasticity*, Prentice-Hall, 3rd edition.

Etrich, C., et. al, 1992, "Dynamics of a Ring-Laser Gyroscope with Backscattering," *Physical review A*, Vol. 46, No. 1 pp. 525~536.

Robert J. Kline-Schoder and Michael J. Wright, 1992, "Design of a Dither Mirror Control System," *Mechanics*, Vol. 2, No. 2, pp. 115~127.

Roy R. Craig, 1981, *Structural Dynamics; An Introduction to Computer Methods*, John Wiley & Sons.

Rudiger rodloff, 1987, "A Laser Gyro with Optimized Resonator Geometry," *IEEE Journal of Quantum Electronics*, Vol. 23, No. 4, pp. 438~445.

Schleich W. and Dobiasch P., 1984, "Noise Analysis of Ring Laser Gyroscope with Arbitrary Dither," *Optics Communications*, Vol. 52, No. 1, pp. 63~68.

Shackleton B. R., 1987, "Mechanical Design Considerations for a Ring Laser Gyro Dither Mechanism," *Proceeding Instrument Mechanical Engineering*, pp. 105~112.

Stephen H. Crandall, Norman C. Dahl and Thomas J. Lardner, 1978, *An Introduction to the Mechanics of Solids*, 2nd, McGraw-Hill, New York.

Stepen P. Timoshenko & James M. Gere, 1963, *Theory of Elastic Stability*, McGraw-Hill, New York, 2nd edition.

Taguchi, K; Fukushima, K; Ishitani, A; Ikeda, M, 1999, "Experimental Investigation of a Semiconductor Ring Laser as an Optical Gyroscope," *IEEE Transactions on Instrumentation and Measurement*, Vol. 48, pp. 1314~1318.

Thomas J. Hutchings, 1978, "Scale Factor Non-Linearity of a Body Dither Laser Gyro," *Proc. IEEE Nat'l Aerospace and Electronic conf.*, pp. 549~555.

Ulrich K. Schreiber et al., 1998, "Precision Stabilization of the Optical Frequency in a Large Ring Laser Gyroscope," *Applied Optics*, Vol. 37, No. 36, pp. 8371~8381.

Vetrov, A. A, 1999, "Calculation, Fabrication, and Study of Waveguides for an Integrated-Optics Gyroscope," *Journal of optical technology*, Vol. 66, No. 5 p. 428.